Electronic Supplementary Material (ESI) for Sustainable Energy & Fuels.

Direct solar to hydrogen conversion enabled by silicon photocathodes with carrier selective passivated contacts

Astha Sharma[1], The Duong[1], Peng Liu[3], Joshua Zheyan Soo[2], Di Yan[1], Doudou Zhang[1], Asim Riaz[2], Christian Samundsett[1], Heping Shen[1], Cheng Yang[3], Siva Krishna Karuturi[1,2*], Kylie Catchpole[1] and Fiona J. Beck[1]*

1. School of Engineering, The Australian National University, Canberra, ACT 2601, Australia

2. Department of Electronic Materials Engineering, ANU Research School of Physics and Engineering, The Australian National University, Canberra, ACT 2601, Australia

3. Division of Energy and Environment, Shenzhen International Graduate School, Tsinghua University, Shenzhen, 518055 China

**Corresponding author-astha.sharma@anu.edu.au, siva.karuturi@anu.edu.au*

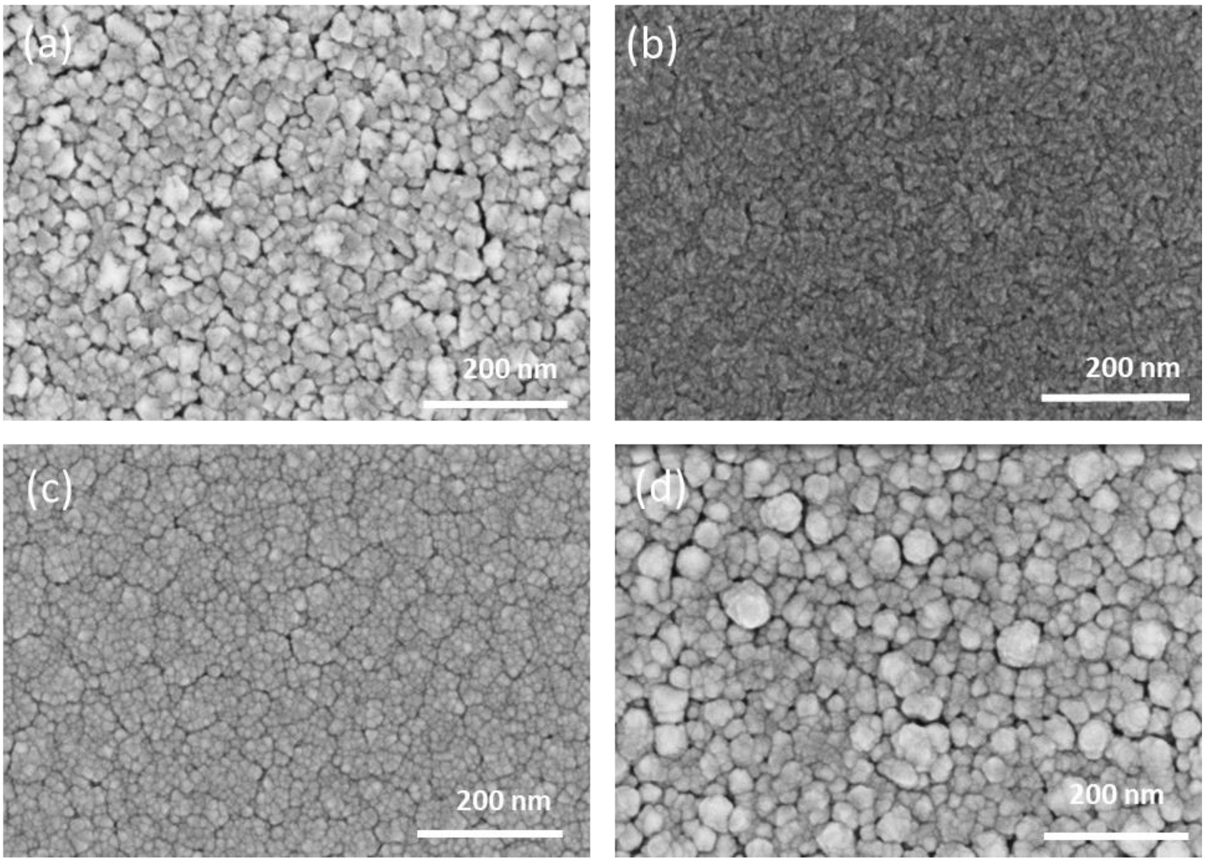

Figure S1. SEM image of (a) Ni (b) Mo (c) NiMo and (d) NiMo/Ni films on SiOx/Si substrate

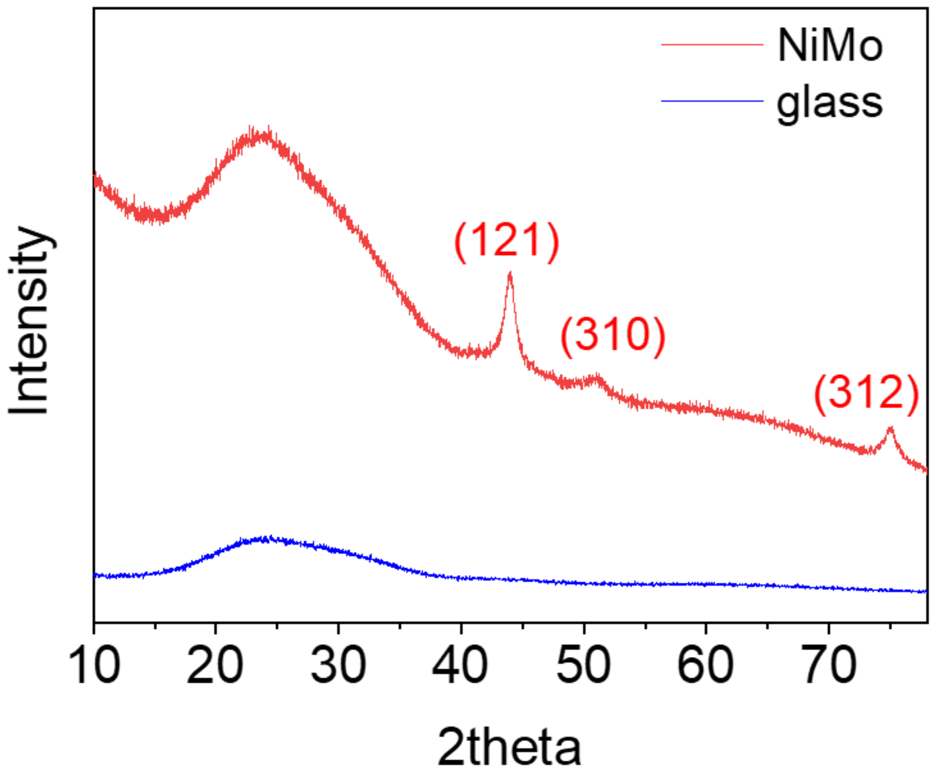

Figure S2. X-ray diffraction of NiMo catalyst on glass substrate.

Table S1. Interplaner spacing (d-spacing) calculations for hkl planes from the XRD.

(hkl)	2 theta	Theta	d-spacing
121	43.5	21.75	2.07
310	51.2	25.6	1.79
312	74.96	37.48	1.26

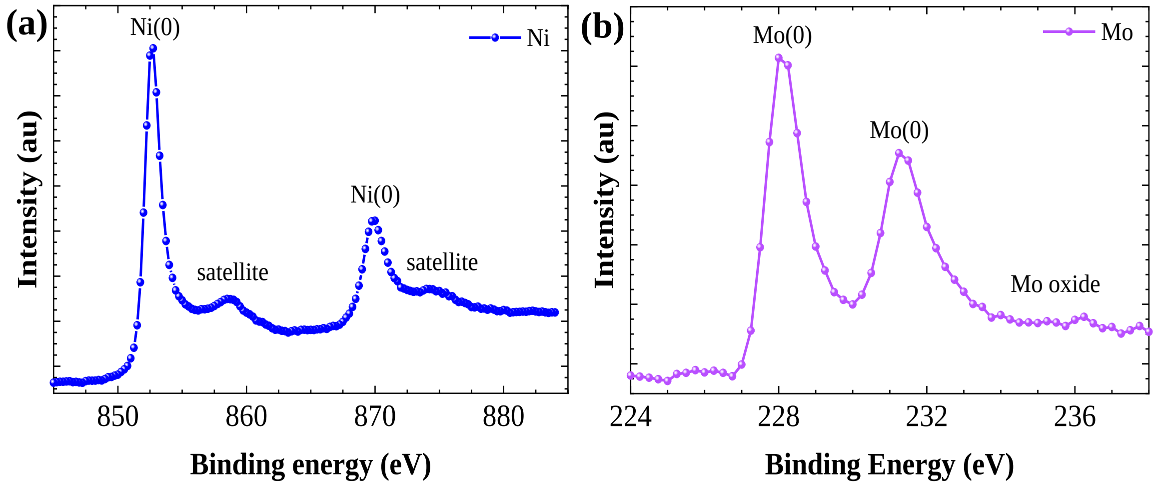

Figure S3. X-ray photoelectron spectra (XPS) of (a) Ni 2p and (b) Mo 3d on Si substrate.

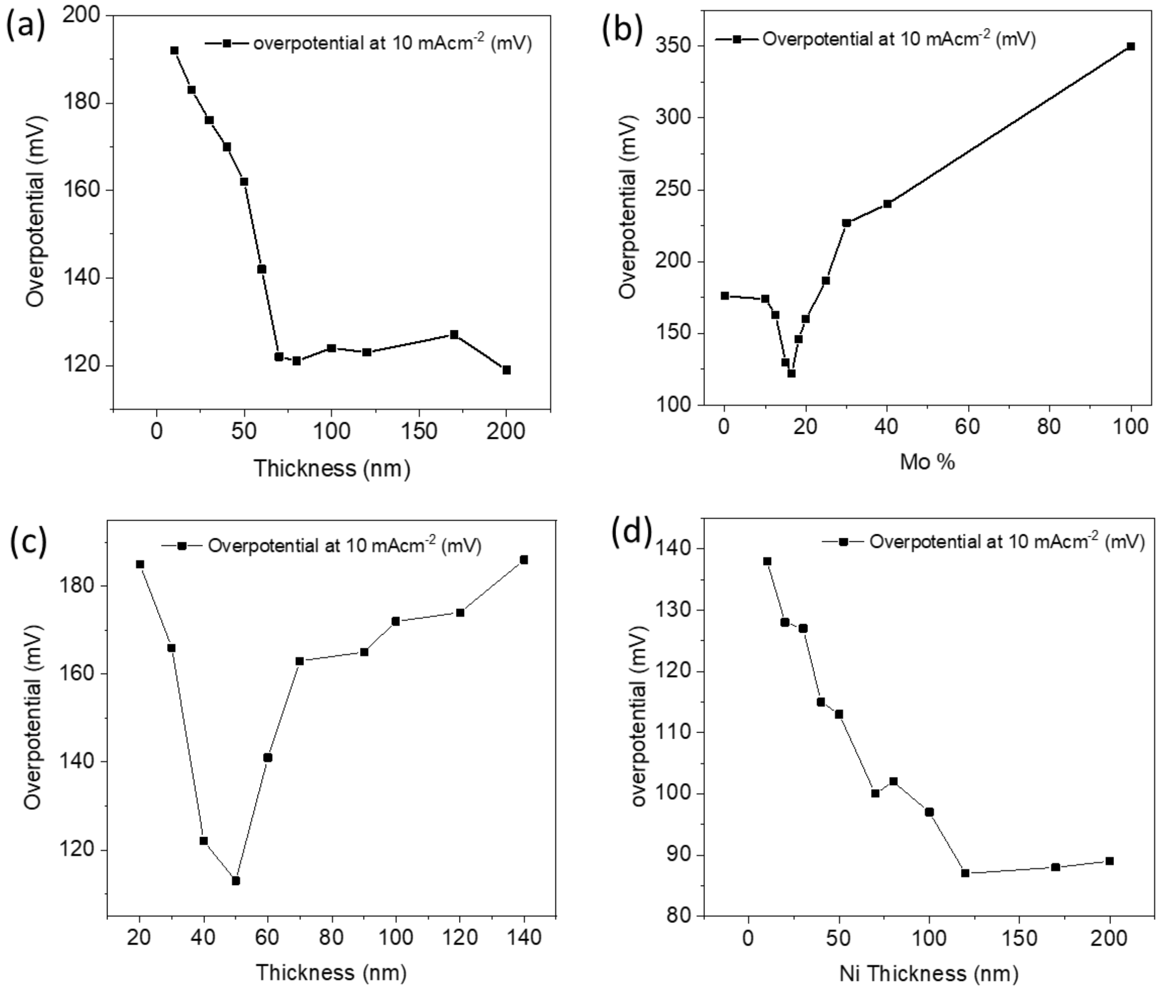

Figure S4. Catalyst thickness and composition optimisation (a) Ni thickness vs overpotential on FTO substrate, (b) NiMo ratio vs overpotential on FTO substrate (fixed thickness), (c) NiMo thickness vs overpotential at optimised ratio on FTO substrate, (d) Ni thickness for Ni/NiMo vs overpotential on FTO substrate (fixed ratio).

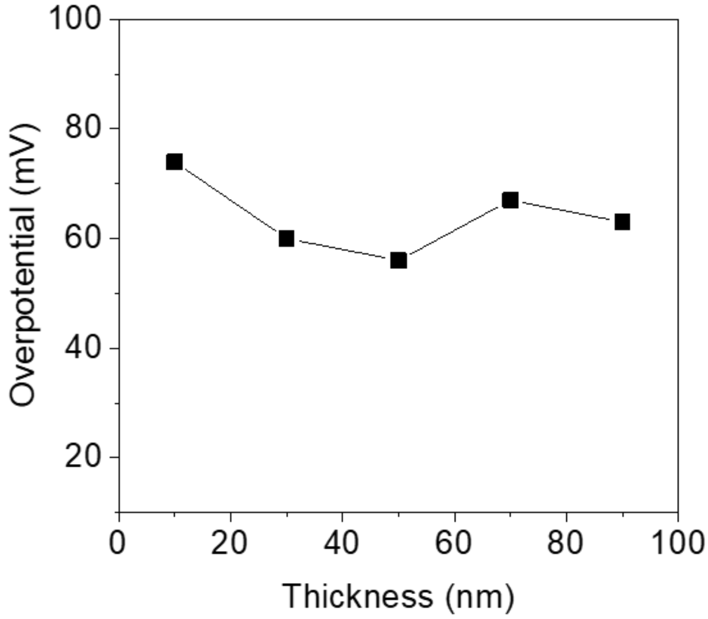

Figure S5. Catalyst thickness optimisation (a) Platinum thickness vs overpotential on FTO substrate

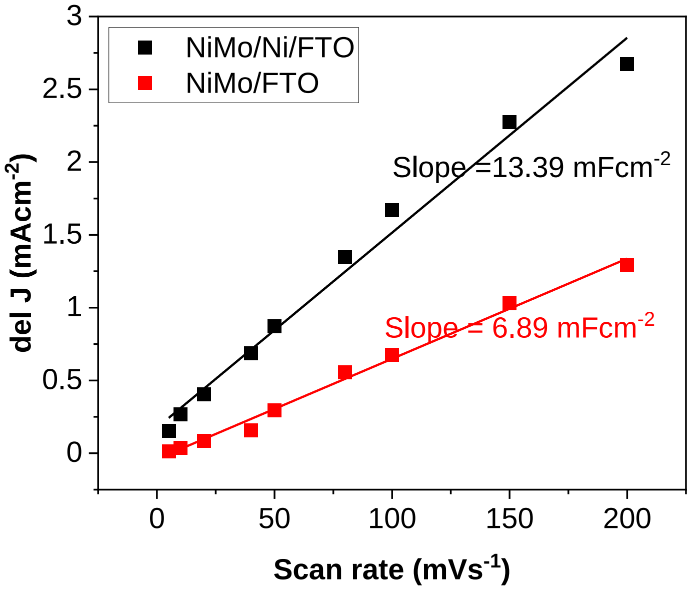

Figure S6. The linear fittings of the capacitive currents of NiMo/Ni/FTO (black) and NiMo/FTO (red) electrodes as a function of scan rate.

Table S2. TCD-FE measurements for NiMo/Ni HER catalyst

Current density	H_2 area	FE_H_2 (Ni/NiMo)
-10	3384	0.97
-10	3460	0.99
-10	3391	0.97
-20	9378	1.02
-20	9176	1.00
-20	9036	0.98
		0.988 = 98.8%

Pt (avg value) of H_2 area for Pt
@ -10 mA – 3469
@ -20 mA - 9140

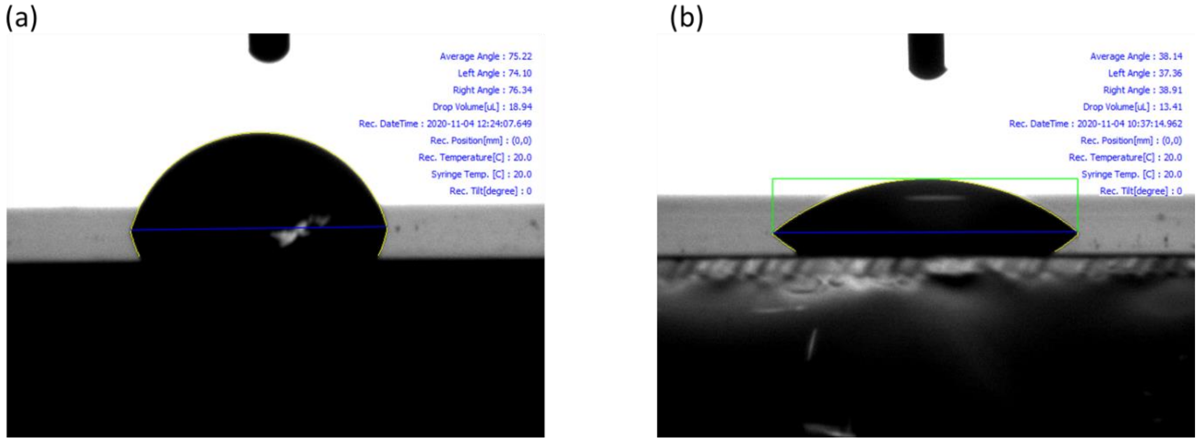

Figure S7. Contact angle measurements of (a) Ni/FTO (b) NiMo/FTO

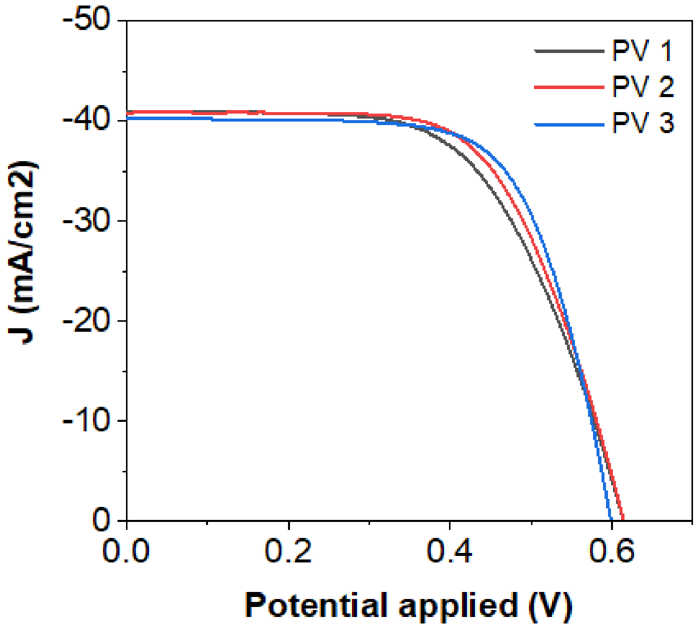

FigureS8. Solid state J-V characteristics of passivated Si PV with 400 nm e-beam deposited Titanium rear contact.

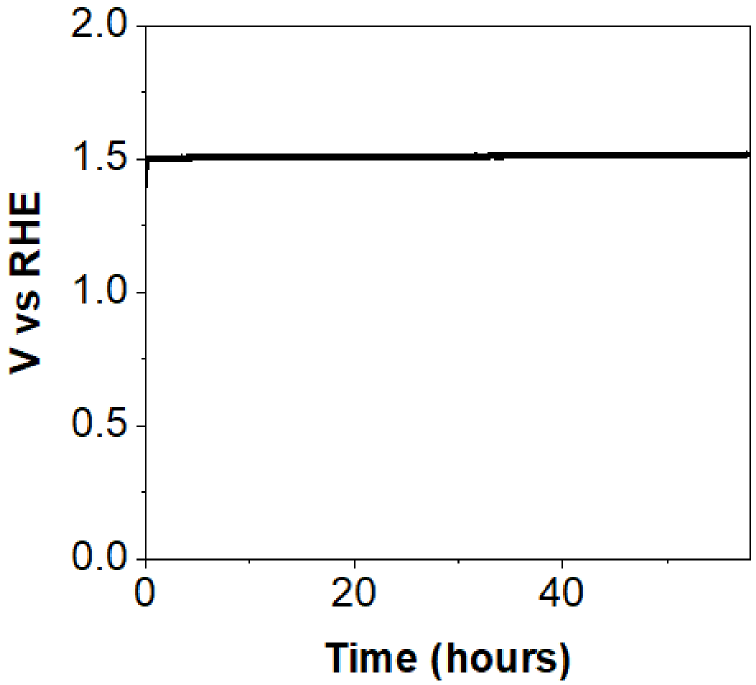

Figure S9. Chronopotentiometry measurements of NiFe nanocone array OER anode in three electrode configuration, 1 M KOH (at J = 30mAcm^{-2})

Table S3. Silicon photocathodes integrated with earth abundant catalysts

Sno	Photo-cathode	Structure	Catalyst deposition technique	ABPE %	ref
1	**p+/n/SiOx/polyn+/Ti/Ni/NiMo**	**Planer**	**Physical deposition – sputter**	**10.5**	**Current work**
2	CoPS/n+pp+Si	Planer	Physical deposition-Metal evaporation	4.7	[1]
3	CoP/n+pSi	Planer	Physical Metal deposition + phosphodization	~4.4	[2]
4	MoSe2/n+pSi	Planer	Physical deposition- Sputtering	3.8	[3]
5	MoS2/Al2O3/n+pSi	Planer	Physical deposition- sputtering	3.6	[4]
6	MoS2/Mo/n+pSi	Planer	Physical Metal deposition + sulfidization	3.1	[5]
7	p+nn+Si/ Ni/ Ni3S2/ MoS2	Planer	Wet chemical- Electrodeposition	11.2	[6]
8	CoWS/Ti/n+pSi	Planer	Wet chemical	4	[7]
9	NiMo /n+pSi	Microwire	Wet chemical- Electrodeposition	10.8	[8]
10	NiMo /NiSi/ n++Si	Microwire	Wet chemical- Electrodeposition	10.1	[9]
11	MoSxCly/n+pp+/Si	Micropyramids	Chemical vapour deposition	6	[10]
12	NiMo/n+pSi	Microwire	Wet chemical- Electrodeposition	1.9	[11]
13	CoP/n+pSi	Microwire	Thermal decomposition	1.9	[12]

Table S4. Unassisted solar water splitting systems with at-least one semiconductor-electrolyte junction and low-cost PV

	PV/Photoelectrode	HER	OER	Catalyst	STH %	Ref
1	**Perovskite PV/Si photocathode**	**NiMo/Ni NiFe**	**NiFe**	**Low-cost**	**17**	**Current Work**
2	Si PV/Si photocathode/Si photoanode	NiMo	Ni	Low-cost	9.8	[13]
3	2Perovskite photoelectrode (series)	CoP	Co3O4	Low-cost	6.7	[14]
4	2 c-Si PV/BiVO4/CoOx photoanode	CoP	Ni	Low-cost	5.3	[15]
5	3 IBC Si (series)	Pt	Ni	High-cost	15.6	[16]
6	a-Si:H/a-Si:H/uC-Si:H	Pt	ZnO:Co	High-cost	9.1	[17]
7	2 c-Si PV/Fe2O3/BiVO4 photoanode	Pt	NiOOH/FeOOH	High-cost	7.7	[18]
8	DSSC PV/WO3/BiVO4 photoanode	Pt	NiOOH/FeOOH	High-cost	7.1	[19]
9	Si photocathode/BiVO4 photoanode	Pt	FeOOH/NiOOH	High-cost	3.7	[20]
10	Perovskite PV/Si photocathode	Pt	IrRu (DSA)	High-cost	17.5	[21]

11	a-Si:H/μc-Si:H/c-Si	Pt	RuO2	High-cost	9.5	[22]
12	Perovskite PV/ CuInGa photocathode		IrRu	High-cost	6.3	[23]
13	DSSC/BiVo4/WO3 photoanode	Pt		High-cost	5.7	[24]

REFERENCES

1. Cabán-Acevedo, M., et al., *Efficient hydrogen evolution catalysis using ternary pyrite-type cobalt phosphosulphide.* Nature materials, 2015. **14**(12): p. 1245-1251.
2. Hellstern, T.R., et al., *Engineering cobalt phosphide (CoP) thin film catalysts for enhanced hydrogen evolution activity on silicon photocathodes.* Advanced Energy Materials, 2016. **6**(4): p. 1501758.
3. Huang, G., et al., *Integrated MoSe2 with n+ p-Si photocathodes for solar water splitting with high efficiency and stability.* Applied Physics Letters, 2018. **112**(1): p. 013902.
4. Fan, R., et al., *Efficient and stable silicon photocathodes coated with vertically standing nano-MoS2 films for solar hydrogen production.* ACS applied materials & interfaces, 2017. **9**(7): p. 6123-6129.
5. Benck, J.D., et al., *Designing active and stable silicon photocathodes for solar hydrogen production using molybdenum sulfide nanomaterials.* Advanced Energy Materials, 2014. **4**(18): p. 1400739.
6. Fan, R., et al., *Highly efficient and stable Si photocathode with hierarchical MoS2/Ni3S2 catalyst for solar hydrogen production in alkaline media.* 2020. **71**: p. 104631.
7. Fan, R., et al., *Efficient n+ p-Si photocathodes for solar H2 production catalyzed by Co-WS and stabilized by Ti buffer layer.* Applied Catalysis B: Environmental, 2018. **237**: p. 158-165.
8. Vijselaar, W., et al., *Spatial decoupling of light absorption and catalytic activity of Ni–Mo-loaded high-aspect-ratio silicon microwire photocathodes.* 2018. **3**(3): p. 185-192.
9. Vijselaar, W., et al., *Efficient and stable silicon microwire photocathodes with a nickel silicide interlayer for operation in strongly alkaline solutions.* ACS energy letters, 2018. **3**(5): p. 1086-1092.
10. Ding, Q., et al., *Designing Efficient Solar-Driven Hydrogen Evolution Photocathodes Using Semitransparent MoQxCly (Q= S, Se) Catalysts on Si Micropyramids.* Advanced Materials, 2015. **27**(41): p. 6511-6518.
11. Warren, E.L., et al., *Hydrogen-evolution characteristics of Ni–Mo-coated, radial junction, n+ p-silicon microwire array photocathodes.* Energy & Environmental Science, 2012. **5**(11): p. 9653-9661.
12. Roske, C.W., et al., *Comparison of the performance of cop-coated and pt-coated radial junction n+ p-silicon microwire-array photocathodes for the sunlight-driven reduction of water to H2 (g).* The journal of physical chemistry letters, 2015. **6**(9): p. 1679-1683.
13. Fan, R., et al., *Unassisted solar water splitting with 9.8% efficiency and over 100 h stability based on Si solar cells and photoelectrodes catalyzed by bifunctional Ni–Mo/Ni.* Journal of Materials Chemistry A, 2019. **7**(5): p. 2200-2209.
14. Liang, J., et al., *A low-cost and high-efficiency integrated device toward solar-driven water splitting.* ACS nano, 2020. **14**(5): p. 5426-5434.
15. Kim, J.H., et al., *A precious metal-free solar water splitting cell with a bifunctional cobalt phosphide electrocatalyst and doubly promoted bismuth vanadate photoanode.* Journal of Materials Chemistry A, 2018. **6**(3): p. 1266-1274.
16. Fu, H.-C., et al., *Spontaneous solar water splitting with decoupling of light absorption and electrocatalysis using silicon back-buried junction.* 2020. **11**(1): p. 1-9.
17. Kirner, S., et al., *Wafer surface tuning for a-Si: H/μc-Si: H/c-Si triple junction solar cells for application in water splitting.* Energy Procedia, 2016. **102**: p. 126-135.
18. Kim, J.H., et al., *Hetero-type dual photoanodes for unbiased solar water splitting with extended light harvesting.* Nature communications, 2016. **7**(1): p. 1-9.
19. Shi, X., et al., *Unassisted photoelectrochemical water splitting exceeding 7% solar-to-hydrogen conversion efficiency using photon recycling.* Nature communications, 2016. **7**(1): p. 1-6.
20. Liu, B., et al., *Double-Side Si Photoelectrode Enabled by Chemical Passivation for Photoelectrochemical Hydrogen and Oxygen Evolution Reactions.* 2020: p. 2007222.
21. Karuturi, S.K., et al., *Over 17% Efficiency Stand-Alone Solar Water Splitting Enabled by Perovskite-Silicon Tandem Absorbers.* Advanced Energy Materials, 2020: p. 2000772.
22. Urbain, F., et al., *Multijunction Si photocathodes with tunable photovoltages from 2.0 V to 2.8 V for light induced water splitting.* Energy & environmental science, 2016. **9**(1): p. 145-154.
23. Luo, J., et al., *Targeting Ideal Dual-Absorber Tandem Water Splitting Using Perovskite Photovoltaics and CuInxGa1-xSe2 Photocathodes.* Advanced Energy Materials, 2015. **5**(24): p. 1501520.

24. Shi, X., et al., *Unassisted photoelectrochemical water splitting beyond 5.7% solar-to-hydrogen conversion efficiency by a wireless monolithic photoanode/dye-sensitised solar cell tandem device.* Nano Energy, 2015. **13**: p. 182-191.